The Origins of Hot Plasma in the Solar Corona

B. De Pontieu, *et al.*

Science **331**, 55 (2011);
DOI: 10.1126/science.1197738

References and Notes

1. D. Li, Y. Xia, *Adv. Mater.* **16**, 1151 (2004).
2. H. Ye, H. Lam, N. Titchenal, Y. Gogotsi, F. Ko, *Appl. Phys. Lett.* **85**, 1775 (2004).
3. M. J. Uddin *et al.*, *J. Photochem. Photobiol. Chem.* **199**, 64 (2008).
4. B. Vigolo *et al.*, *Science* **290**, 1331 (2000).
5. M. E. Kozlov *et al.*, *Adv. Mater.* **17**, 614 (2005).
6. M. Zhang, K. R. Atkinson, R. H. Baughman, *Science* **306**, 1358 (2004).
7. M. Zhang *et al.*, *Science* **309**, 1215 (2005).
8. X. Zhang *et al.*, *Adv. Mater.* **18**, 1505 (2006).
9. Q. Li *et al.*, *Adv. Mater.* **18**, 3160 (2006).
10. X. Zhang *et al.*, *Small* **3**, 244 (2007).
11. L. Xiao *et al.*, *Appl. Phys. Lett.* **92**, 153108 (2008).
12. Y. Nakayama, *Jpn. J. Appl. Phys.* **47**, 8149 (2008).
13. A. E. Aliev *et al.*, *Science* **323**, 1575 (2009).
14. Materials and methods are available as supporting material on *Science* Online.
15. D. Golberg, Y. Bando, C. Tang, C. Zhi, *Adv. Mater.* **19**, 2413 (2007).
16. V. M. Castaño, *Jpn. J. Appl. Phys.* **44**, 5009 (2005).
17. J. Nagamatsu, N. Nakagawa, T. Muranaka, Y. Zenitani, J. Akimitsu, *Nature* **410**, 63 (2001).
18. S. X. Dou *et al.*, *Adv. Mater.* **18**, 785 (2006).
19. D. V. Kosynkin *et al.*, *Nature* **458**, 872 (2009).
20. D. A. Dikin *et al.*, *Nature* **448**, 457 (2007).
21. T. Bhardwaj, A. Antic, B. Pavan, V. Barone, B. D. Fahlman, *J. Am. Chem. Soc.* **132**, 12556 (2010).
22. A. K. Padhi, K. S. Nanjundaswamy, J. B. Goodenough, *J. Electrochem. Soc.* **144**, 1188 (1997).
23. J. Chen, M. S. Whittingham, *Electrochem. Commun.* **8**, 855 (2006).
24. X. Li, F. Kang, X. Bai, W. Shen, *Electrochem. Commun.* **9**, 663 (2007).
25. A. B. Dalton *et al.*, *Nature* **423**, 703 (2003).
26. K. Gong, F. Du, Z. Xia, M. Durstock, L. Dai, *Science* **323**, 760 (2009).
27. S. Kundu *et al.*, *J. Phys. Chem. C* **113**, 14302 (2009).
28. S. Maldonado, K. J. Stevenson, *J. Phys. Chem. B* **109**, 4707 (2005).
29. Y. Shao, J. Sui, G. Yin, Y. Gao, *Appl. Catal. B* **79**, 89 (2008).
30. M. Terrones, R. Kamalakaran, T. Seeger, M. Rühle, *Chem. Commun. (Camb.)* **23**, 2335 (2000).

31. We thank A. L. Elias and M. Terrones for N-doped MWNTs; D. Goldberg and Y. Bando for boron nitride nanotubes; E. J. Kneeland, A. E. Nabinger, S. Y. Yoon, and M. J. de Andrade for help with experiments; and A. E. Aliev and D. M. Rogers for useful comments. Supported by Air Force Grant AOARD-10-4067, Air Force Office of Scientific Research grants FA9550-09-1-0384 and FA9550-09-1-0537, Office of Naval Research Multidisciplinary University Research Initiative grant N00014-08-1-0654, NSF grant DMI-0609115, and Robert A. Welch Foundation grant AT-0029. Some of the authors have filed patent application PCT/US2010/36378 (27 May 2010).

Supporting Online Material

www.sciencemag.org/cgi/content/full/331/6013/51/DC1
Materials and Methods
Figs. S1 to S7
References
Movies S1 to S3

2 August 2010; accepted 26 November 2010
10.1126/science.1195912

The Origins of Hot Plasma in the Solar Corona

B. De Pontieu,[1]* S. W. McIntosh,[2] M. Carlsson,[3] V. H. Hansteen,[3,1] T. D. Tarbell,[1] P. Boerner,[1] J. Martinez-Sykora,[1,3] C. J. Schrijver,[1] A. M. Title[1]

The Sun's outer atmosphere, or corona, is heated to millions of degrees, considerably hotter than its surface or photosphere. Explanations for this enigma typically invoke the deposition in the corona of nonthermal energy generated by magnetoconvection. However, the coronal heating mechanism remains unknown. We used observations from the Solar Dynamics Observatory and the Hinode solar physics mission to reveal a ubiquitous coronal mass supply in which chromospheric plasma in fountainlike jets or spicules is accelerated upward into the corona, with much of the plasma heated to temperatures between ~0.02 and 0.1 million kelvin (MK) and a small but sufficient fraction to temperatures above 1 MK. These observations provide constraints on the coronal heating mechanism(s) and highlight the importance of the interface region between photosphere and corona.

A wide variety of theoretical models to explain the heating of the solar corona have been proposed since the discovery in the corona of emission from ions that are formed at temperatures of several million kelvin (MK) (*1*). These models range from energy deposition through the damping of magnetohydrodynamic waves, to nanoflares (*2*) that arise when the magnetic field is stressed (via reconnection) (*3*). Despite decades of effort to determine which mechanism dominates, the lack of detailed observations of the fundamental heating process has hampered progress. Instead, most efforts have focused on statistical approaches that study the dependence of the heating mechanism on magnetic field strength, loop length, or plasma density (*4*), or that are based on assumptions about unresolved individual heating events (*5*).

Spicules are phenomena that have held particular promise as discrete coronal heating events (*6*, *7*). The chromospheric mass flux that these jets propel to coronal heights is estimated to be two orders of magnitude larger than the mass flux of the solar wind (*8*). Although they have been observed in a variety of chromospheric and transition region (TR) lines (*9*, *10*), a coronal counterpart has not been observed. As a result, a role for spicules in coronal heating has been dismissed as unlikely (*8*). On the other hand, recent observations have revealed a new type of spicule that is shorter-lived (~100 s) and more dynamic (~50 to 100 km/s) than its classical counterpart (*10*, *11*). Recently, a spatiotemporal correlation between chromospheric brightness changes, suggestively linked to these "type II" spicules, and coronal upflows of 50 to 100 km/s, deduced from spectral line asymmetries of coronal lines at the footpoints of loops, was found (*12*). This statistical relationship suggests that the chromospheric jets may play a substantial role in providing the corona with hot plasma, but a detailed one-to-one correlation between spicules and their coronal counterparts has remained elusive (*10*, *11*, *13*).

We exploited the recent detection of the disk counterpart of type II spicules: rapid blueshifted events (RBEs), which are observed in chromospheric lines such as Hα 6563 Å (*14*, *15*). Observations suggest evidence for acceleration and heating along their long axis before they rapidly fade out of the chromospheric passbands, which may indicate heating to TR temperatures (*15*). We used coordinated observations of RBEs in the blue wing of Hα (–0.868 Å or –41 km/s) with the Narrowband Filter Imager of the Solar Optical Telescope (SOT) (*17*) onboard the Hinode solar physics mission (*16*), and found direct evidence of a strong correlation of RBEs with short-lived brightenings in a wide range of TR and coronal passbands observed with the Atmospheric Imaging Assembly (AIA) onboard the recently launched Solar Dynamics Observatory (SDO). Using an automated detection code, we found 2434 RBEs occurring in the active-region plage footpoints of coronal loops during a 1-hour-long time series (*18*) on 25 April 2010 (Fig. 1 and fig. S1).

RBEs form rapidly and often recur in the same position (Fig. 2). They become visible as an absorbing feature in the upper chromospheric Hα line that is blueshifted by 40 to 60 km/s along the line of sight (*18*). A little bit later, brightenings occur in the vicinity of the leading edge of the RBE in the He II 304 Å, Fe IX 171 Å, and Fe XIV 211 Å AIA passbands (Fig. 2). These passbands are dominated by lines from ions that are formed at temperatures of 0.1, 0.8, and 2 MK, respectively (*18*). The extreme ultraviolet emission moves at velocities similar to those of the leading end of the RBE, although the emission in He II 304 Å (and sometimes Fe IX 171 Å) often,

[1]Lockheed Martin Solar and Astrophysics Laboratory, 3251 Hanover Street, Organization ADBS, Building 252, Palo Alto, CA 94304, USA. [2]High Altitude Observatory, National Center for Atmospheric Research, Post Office Box 3000, Boulder, CO 80307, USA. [3]Institute of Theoretical Astrophysics, University of Oslo, Post Office Box 1029 Blindern, 0315 Oslo, Norway.

*To whom correspondence should be addressed. E-mail: bdp@lmsal.com

sometimes with a short delay, fills in along the whole length of the RBE, usually after the RBE disappears out of the chromospheric passband (movies S2 to S7). Space-time plots show that the apparent velocity of the chromospheric, TR, and coronal signals is similar, with typical velocities on the order of 50 to 100 km/s (Fig. 2 and fig. S2).

The location of the hot plasma with respect to the chromospheric RBE varies substantially as a function of temperature *T*, with a clear displacement of the hottest emission toward locations ahead of the leading edge of the RBE (in a vertical geometry this would be "upward from the RBE"). The hotter Fe XIV emission often occurs over a larger spatial range than the other TR and coronal lines, usually protruding ahead of the RBE for a few megameters (Mm) (fig. S2 and movies S4 and S5). This may be caused by the effects of thermal conduction, which is much more efficient at Fe XIV temperatures, given its temperature dependence ($T^{3.5}$). Thermal conduction is clearly not the only cause for the "upward" extension of the coronal emission associated with RBEs: The presence of strong line-of-sight Doppler velocities in the chromosphere, and the compatible apparent velocities of the coronal brightenings moving along with the RBEs, show that the apparent motion of the coronal brightenings is associated with strong mass flows on the order of 50 to 100 km/s. This is confirmed by the presence (in regions with RBE activity) of blueward asymmetries (*18*) in the Si VII 275 Å spectral line profiles from the Extreme Ultraviolet Imaging Spectrometer (EIS) (*19*) onboard Hinode (Fig. 1). Such asymmetries have been linked to a faint secondary component of strongly upflowing (50 to 100 km/s) coronal plasma (*12*, *20*).

The heating of plasma to coronal temperatures in association with spicules is ubiquitous: We find evidence for a similar process in active regions, in the quiet Sun, and in coronal holes (figs. S3 to S5). In particular, chromospheric spicules (observed with Hinode's SOT in Ca II H 3968 Å) at the limb in coronal holes are intimately linked to the formation of features at TR and coronal temperatures (Fig. 3). The spicules show strong apparent upward motions on the order of 50 100 km/s before rapidly fading out of the chromospheric passband (movies S8 and S9). Using coaligned AIA images, we find that the fading of chromospheric spicules is directly linked

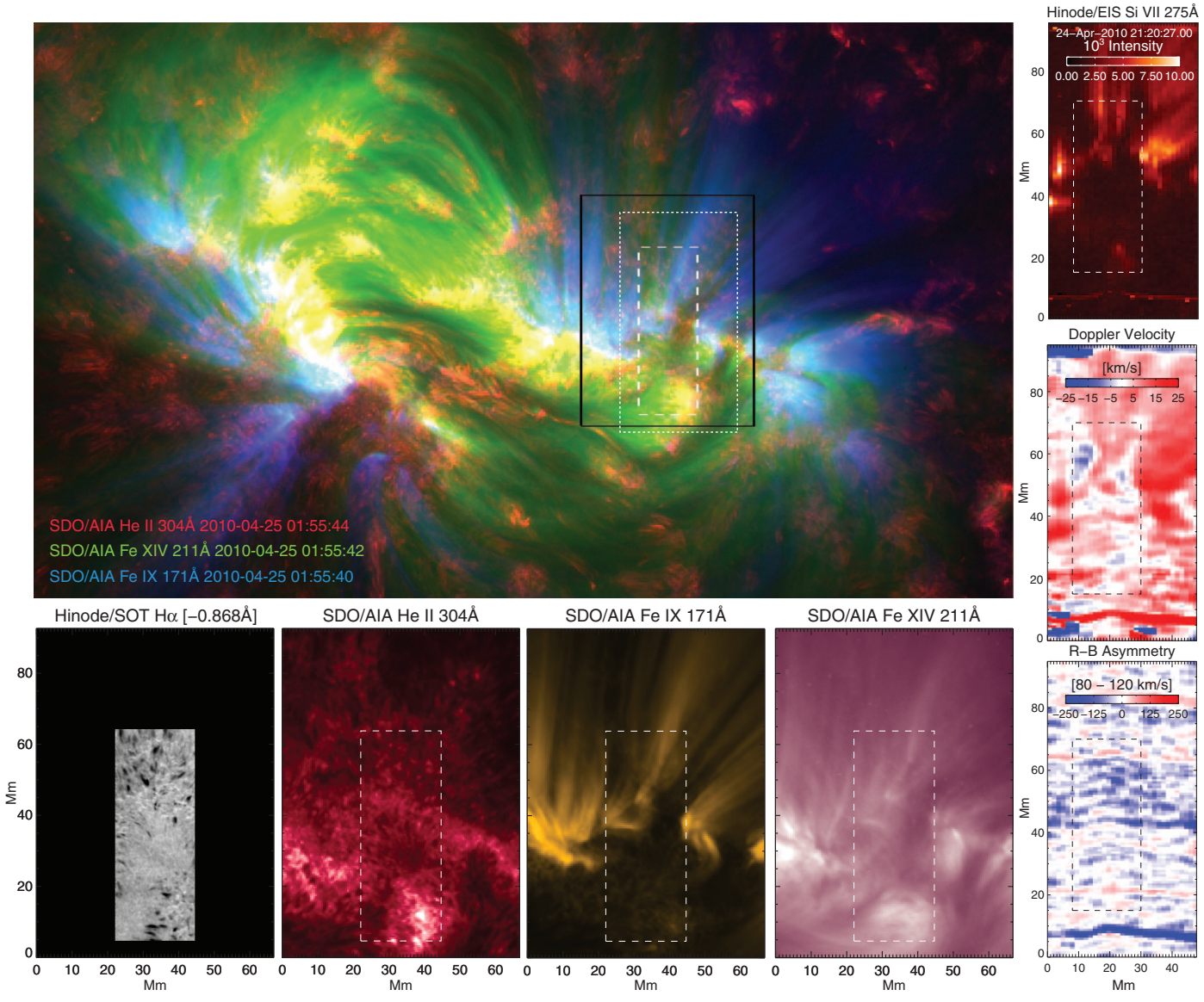

Fig. 1. The chromosphere, TR, and corona of the active region studied on 25 April 2010 (see fig. S1 and movies S1 to S3). (**Upper panel**) A composite layering with He II 304 Å (red, 0.1 MK), Fe XIV 211 Å (green, 2 MK), and Fe IX 171 Å (blue, 0.8 MK) images from AIA. (**Bottom row**) RBEs in Hα –0.868 Å (lower left) throughout the SOT field of view (white/black dashed lines in other panels), and AIA images for the region of interest (solid black line in top panel). (**Right column**) Si VII 275 Å EIS spectral raster (outlined by dotted line in top left panel) taken a few hours before with intensity (top), Doppler shift (middle), and blueward asymmetries at velocities of 80 to 120 km/s (bottom).

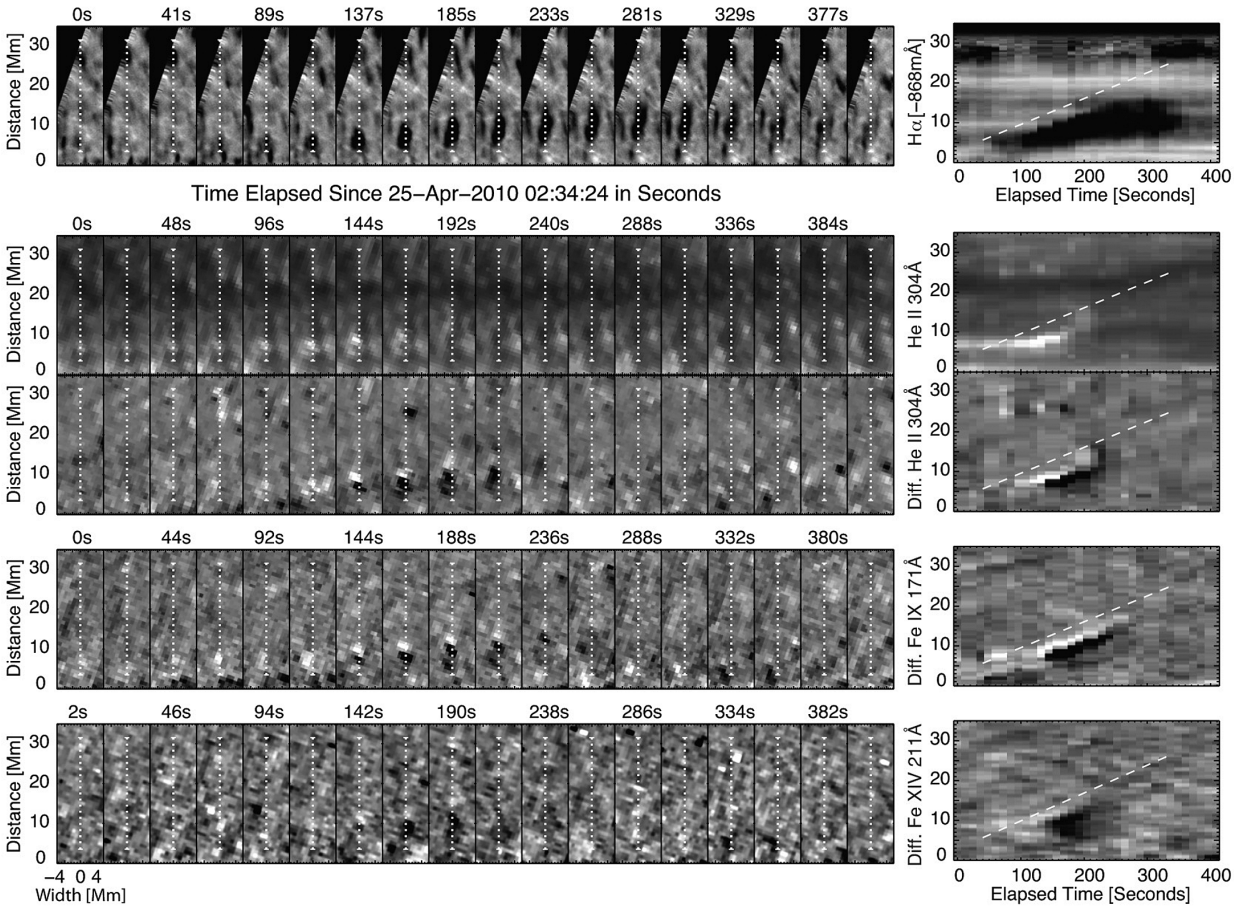

Fig. 2. Typical dynamic and thermal evolution of a succession of RBEs. (**Left panels, top to bottom**) The temporal evolution of Hα –0.868 Å, He II 304 Å intensity, and the running time-difference time series (*18*) (32 s) for He II 304 Å, Fe IX 171 Å, and Fe XIV 211 Å. (**Right panels, top to bottom**) Space-time plots along the axis of the RBE (dotted white lines) for the same passbands, with a dashed guideline to illustrate speeds of 70 km/s. See fig. S2 for another example and movies S2 to S7.

Fig. 3. Typical dynamic and thermal evolution of type II spicules at the coronal hole limb on 27 April 2010. The top panels show, from top to bottom, the temporal evolution of a succession of type II spicules visible as jetlike features in Ca II H 3968 Å and He II 304 Å, and as absorbing features at the bottom and streaklike brightenings at the spicule tops in Fe IX 171 Å. Space-time plots along the line connecting the black and white short lines (at top and bottom of top panels) for the intensity (lower left panels; for the 171 Å panel, the time average has been subtracted) and the running time difference (40 s, lower right panels) show rapid upflows and fading at heights below 15 Mm (marked by crosses in the lower panels) for Ca II, followed by parabolic paths up to heights of 20 to 25 Mm for He II 304 Å and upward-propagating disturbances in Fe IX 171 Å (visible in running time-difference panels). A detailed, annotated description of the sequence of events in this figure is available as movie S8. See also figs. S4 and S5 and movie S9.

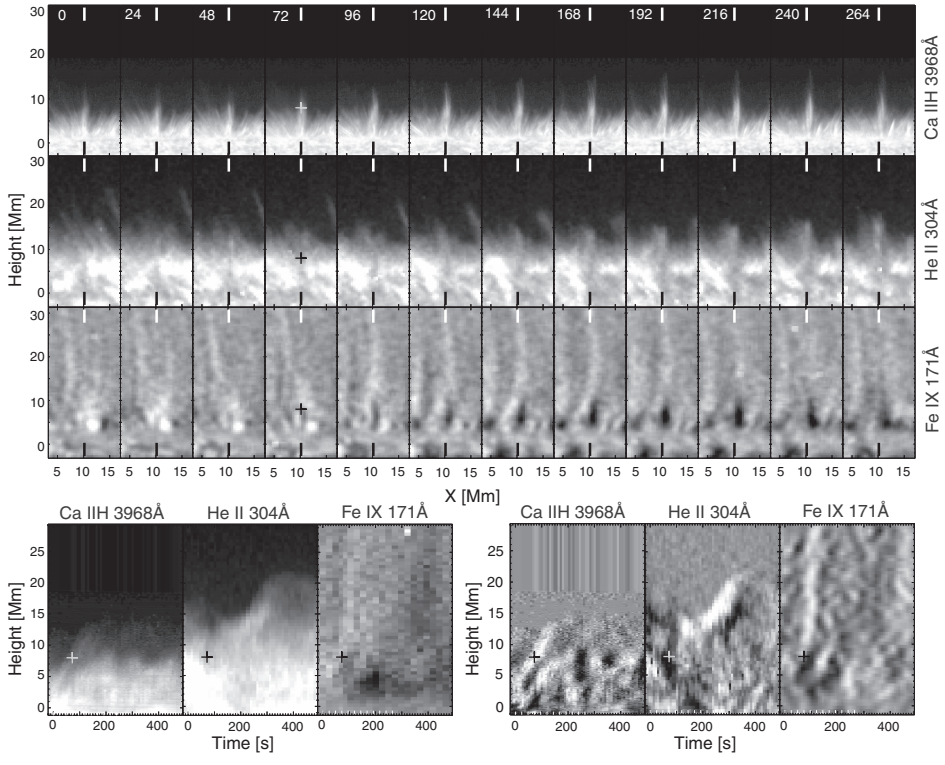

to the formation of spicular features in He II 304 Å (~0.1 MK). These TR spicules appear with a time delay of around 10 to 20 s, reach much larger heights (~10 to 20 Mm), and typically fall back to the surface within a matter of several minutes, following a parabolic path (Fig. 3 and fig. S5). Despite the enormous line-of-sight superposition at the limb, we often also observe a coronal counterpart of chromospheric/TR spicules (Fig. 3 and fig. S5) in the Fe IX 171 Å images. At the bottom, this takes the form of a dark feature that corresponds to the bright Ca II H feature (movie S8), likely from continuum absorption from neutral hydrogen and helium (*21*). During the later stages, the dark feature disappears (likely because heating reduces the amount of neutral hydrogen and helium), and bright coronal counterparts propagate upward into the coronal hole with similar velocities as the apparent motions of the chromospheric spicules (fig. S5). These coronal counterparts appear to be related to the propagating disturbances in coronal holes that have previously been interpreted as waves (*22*) and more recently linked to upflows (*23*, *24*).

Our observations support a scenario in which chromospheric plasma is propelled upward with speeds of ~50 to 100 km/s, with the bulk of the mass rapidly heated to TR temperatures (~0.02 to 0.1 MK), after which it returns to the surface (invisible to chromospheric passbands). Directly associated with these jets, plasma is heated to coronal temperatures of at least 1 to 2 MK, at the bottom during the initial stages, and both along and toward the top of the chromospheric feature later on. The coronal counterparts of the jets are seen to rapidly propagate upward, likely as a result of strong upflows and/or thermal conduction or waves. Based on the ubiquity of these events and the observed coronal intensities, we estimate that these events carry a mass flux density of 1.5×10^{-9} g/cm^2/s and an energy flux density of $\sim 2 \times 10^6$ erg/cm^2/s into the corona (*25*). This is of the order that is required to sustain the energy lost from the active-region corona (*26*). Given the conservative nature of our estimate, these events are likely to play a substantial role in the coronal energy balance.

Although early models have implicated the heating of chromospheric spicules in the coronal heating problem (*6*), the detailed thermal and spatiotemporal evolution we observed is not compatible with any of the well-established models for coronal heating: None of those predict such strong upflows (driven from below) at chromospheric temperatures (*2*, *27*). These models typically assume energy deposition in the corona, which leads to heating and evaporation of plasma from the chromospheric mass reservoir, driven by thermal conduction from above. Recent advanced numerical models do predict heating rates per particle that reach their maximum in the upper chromosphere (*28*, *29*), which is compatible with our observations. Some analytical models also suggest that dissipation of current sheets resulting from the shuffling of ubiquitous mixed-polarity fields on small scales can provide coronal heating at low heights (*30*). However, there are currently no models for what drives and heats the observed jets (*31*). These first detailed observations of individual coronal heating events highlight the importance of the chromosphere and magnetohydrodynamic/plasma physics approaches for a better understanding of heating in the solar atmosphere.

References and Notes

1. B. Edlen, *Z. Astrophysik* **22**, 30 (1942).
2. J. A. Klimchuk, *Sol. Phys.* **234**, 41 (2006).
3. E. N. Parker, *Geophys. Astrophys. Fluid Dyn.* **50**, 229 (1990).
4. C. J. Schrijver, A. W. Sandman, M. J. Aschwanden, M. L. DeRosa, *Astrophys. J.* **615**, 512 (2004).
5. M. J. Aschwanden, R. Nightingale, P. Boerner, *Astrophys. J.* **656**, 577 (2007).
6. G. W. Pneuman, R. A. Kopp, *Sol. Phys.* **57**, 49 (1978).
7. R. G. Athay, T. E. Holzer, *Astrophys. J.* **255**, 743 (1982).
8. G. L. Withbroe, *Astrophys. J.* **267**, 825 (1983).
9. K. P. Dere, J.-D. F. Bartoe, G. E. Brueckner, *Sol. Phys.* **123**, 41 (1989).
10. R. Rutten, *ASP Conf. Ser.* **354**, 276 (2006)
11. B. De Pontieu *et al.*, *Pub. Astron. Soc. Jpn.* **59**, 655 (2007).
12. B. De Pontieu, S. W. McIntosh, V. H. Hansteen, C. J. Schrijver, *Astrophys. J.* **701**, L1 (2009).
13. J. Mariska, *Solar Transition Region* (Cambridge Astrophysics Series, vol. 23, Cambridge Univ. Press, New York, 1992).
14. Ø. Langangen *et al.*, *Astrophys. J.* **679**, L167 (2008).
15. L. Rouppe van der Voort, J. Leenaarts, B. de Pontieu, M. Carlsson, G. Vissers, *Astrophys. J.* **705**, 272 (2009).
16. T. Kosugi *et al.*, *Sol. Phys.* **243**, 3 (2007).
17. S. Tsuneta *et al.*, *Sol. Phys.* **249**, 167 (2008).
18. See materials and methods in the supporting online material (SOM) on *Science* Online.
19. J. L. Culhane *et al.*, *Sol. Phys.* **243**, 19 (2007).
20. H. Hara *et al.*, *Astrophys. J.* **678**, L67 (2008).
21. U. Anzer, P. Heinzel, *Astrophys. J.* **622**, 714 (2005).
22. D. Banerjee *et al.*, *Astron. Astrophys.* **499**, 29 (2009).
23. S. W. McIntosh, B. De Pontieu, *Astrophys. J.* **707**, 524 (2009).
24. S.W. McIntosh *et al.*, *Astron. Astrophys.* **510**, 2 (2010).
25. See SOM discussion.
26. E. R. Priest, *Solar Magnetohydrodynamics* (D. Reidel Publishing, Dordrecht, Netherlands, 1982).
27. S. Patsourakos, J. A. Klimchuk, *Astrophys. J.* **647**, 1452 (2006).
28. B. V. Gudiksen, A. Nordlund, *Astrophys. J.* **618**, 1031 (2005).
29. V. H. Hansteen, H. Hara, B. De Pontieu, M. Carlsson, *Astrophys. J.* **718**, 1070 (2010).
30. E. Priest, J. Heyvaerts, A. Title, *Astrophys. J.* **576**, 533 (2002).
31. A. Sterling, *Sol. Phys.* **196**, 79 (2000).

32. This work is supported by NASA grants NNX08AL22G and NNX08BA99G (to B.D.P. and S.W.M.), NASA contracts NNM07AA01C (Hinode) and NNG04EA00C (AIA), and the Research Council of Norway (M.C. and V.H.H.). The National Center for Atmospheric Research is sponsored by NSF. Hinode is a Japanese mission developed by the Institute of Space and Astronautical Science/Japan Aerospace Exploration Agency, with the National Astronomical Observatory of Japan as domestic partner and NASA and Science and Technology Facilities Council (UK) as international partners. It is operated in cooperation with the European Space Agency and the Norwegian Space Centre (Norway).

Supporting Online Material

www.sciencemag.org/cgi/content/full/331/6013/55/DC1
Materials and Methods
SOM Text
Figs. S1 to S5
References
Movies S1 to S9

13 September 2010; accepted 2 December 2010
10.1126/science.1197738

Universal Quantum Viscosity in a Unitary Fermi Gas

C. Cao,[1] E. Elliott,[1] J. Joseph,[1] H. Wu,[1] J. Petricka,[2] T. Schäfer,[3] J. E. Thomas[1]*

A Fermi gas of atoms with resonant interactions is predicted to obey universal hydrodynamics, in which the shear viscosity and other transport coefficients are universal functions of the density and temperature. At low temperatures, the viscosity has a universal quantum scale $\hbar n$, where n is the density and $\hbar$ is Planck's constant h divided by 2π, whereas at high temperatures the natural scale is $p_T^3/\hbar^2$, where p_T is the thermal momentum. We used breathing mode damping to measure the shear viscosity at low temperature. At high temperature T, we used anisotropic expansion of the cloud to find the viscosity, which exhibits precise $T^{3/2}$ scaling. In both experiments, universal hydrodynamic equations including friction and heating were used to extract the viscosity. We estimate the ratio of the shear viscosity to the entropy density and compare it with that of a perfect fluid.

Ultracold, strongly interacting Fermi gases are of broad interest because they provide a tunable tabletop paradigm for strongly interacting systems, ranging from high-temperature superconductors to nuclear matter. First observed in 2002, quantum degenerate, strongly interacting Fermi gases are being widely studied (*1*–*4*). To obtain strong interactions (characterized by a divergent s-wave scattering length), a bias magnetic field is used to tune the gas to a broad collisional (Feshbach) resonance, for which the range of the collision potential is small compared with the interparticle spacing. In this so-called unitary regime, the properties of the gas are universal functions of the density n and temperature T. The universal behavior of the equilibrium thermodynamic properties has been studied in detail (*5*–*11*), whereas the measurement of universal transport coefficients presents new challenges.

[1]Department of Physics, Duke University, Durham, NC 27708, USA. [2]Department of Physics, Gustavus Adolphus College, Saint Peter, MN 56082, USA. [3]Department of Physics, North Carolina State University, Raleigh, NC 27695, USA.

*To whom correspondence should be addressed. E-mail: jet@phy.duke.edu